Solid State Communications 250 (2017) 84–91

Contents lists available at ScienceDirect

Solid State Communications

journal homepage: www.elsevier.com/locate/ssc

Communication

Electronic heat capacity and magnetic susceptibility of ferromagnetic silicene sheet under strain

Mohsen Yarmohammadi

Young Researchers and Elite Club, Kermanshah Branch, Islamic Azad University, Kermanshah, Iran

ARTICLE INFO

Keywords:
Ferromagnetic silicene
Green's function
Strain
Electronic heat capacity
Magnetic susceptibility
Electric field

ABSTRACT

The electronic heat capacity (EHC) and magnetic susceptibility (MS) of the two-dimensional material ferromagnetic graphene's silicon analog, silicene, are investigated by the strain-induced and the applied electric field within the Green's function technique and the Kane-Mele Hamiltonian. Dirac cone approximation has been performed to investigate the system under strain along the zigzag (ZZ) direction. The main attention is focused on the effects of external static electric field in the presence of strain on EHC and MS of a ferromagnetic silicene sheet. In the presence of strain, carriers have a larger effective mass and transport decreases. As a result, the temperature dependence of EHC and MS gives a critical strain around 10%. Furthermore, electric field breaks the reflection symmetry of the structure and a transition to the topological insulator for strained ferromagnetic silicene has occurred when the electric field is increased. In this phase, EHC and MS have weird behaviors with temperature.

1. Introduction

After the discovery of first real 2D-material graphene in 2004 [1], significant interest has been attracted in studying physical properties of 2D-materials both experimentally and theoretically with the honeycomb lattices such as hexagonal boron-nitride ($h-BN$), MoS_2 and recently a monolayer of silicon, known as silicene. Although these materials have a honeycomb lattice, but their properties are different [2–6]. In graphene, there is a minimal conductivity in the limit of zero doping, i.e., at Dirac points (K and K') which this can be understood because of its linear dispersion energy in the vicinity of K and K' valleys of the Brillouin zone [7,8]. This minimal conductivity creates a problem for using graphene as a highly motivated new material in electronic devices and electrical conduction can not be switched off by using the control voltages [9], which is essential for the operation of conventional transistors. One of the ways to overcome this problem is the creation of band gap in graphene electronic band structure which is made by inversion symmetry breaking [10,11]. It is desirable to have band gap in materials in addition to their novel features. Unlike graphene, according to the Fig. 1, silicene has a hexagonal atomic arrangement but due to its large ionic radius has a buckled configuration such that its sublattices (A and B) sit in two parallel planes with a vertical distance 0.46 nm [12–17]. The low-energy dynamics of fermions in graphene is described by the Dirac Hamiltonian for both valleys, but in silicene due to the strong spin-orbit (SO) interaction, carriers are massive with an energy gap around 1.55 meV [18,19]. This gap can be induced via an applied perpendicular electric field to its layer which leads to the many attractive properties of silicene [20–27]. The strain can change many features of 2D-materials. In graphene, Dirac points remain at K and K' points under biaxial strain, but they affected for strain along the different directions [28–31]. Contrary to the graphene, both the σ^* and π^* bands in silicene are more sensitive to the strain-induced [32–36]. For example, silicene becomes metallic under biaxial strain larger than 12% [32–34] and it turns into a metal under strain larger than 12% (14%) along the AC (ZZ) directions [36]. However, the investigation of thermodynamic properties of silicene under strain is still remain to be studied.

Unlike electronic properties, the thermal properties of silicence are still not well studied. Many works have been done in this case. For example, thermal conductivity of silicene is predicted around 20–65 W/mK [37–41]. The EHC of a semiconductor system is defined as the ratio of that portion of the heat used by the carriers (here, Dirac fermions) to the rise in temperature of the system. On the other hand, MS is the degree of magnetization of a material in response to an applied magnetic field. Our system is considered as ferromagnetic with an exchange field M. In this work, we have investigated the temperature dependence of EHC and MS in a ferromagnetic silicene sheet under strain at Dirac points., at a fixed strain modulus and direction of applied strain, EHC and MS are studied with electric field. Green's function approach is carried out within the Kane-Mele Hamiltonian. The outline of this paper is as follows: Section 2 describes the Hamiltonian and theoretical formalism. In Section 3, we show the

E-mail address: m.yarmohammadi69@gmail.com.

http://dx.doi.org/10.1016/j.ssc.2016.11.019
Received 13 May 2016; Received in revised form 6 October 2016; Accepted 24 November 2016
Available online 27 November 2016

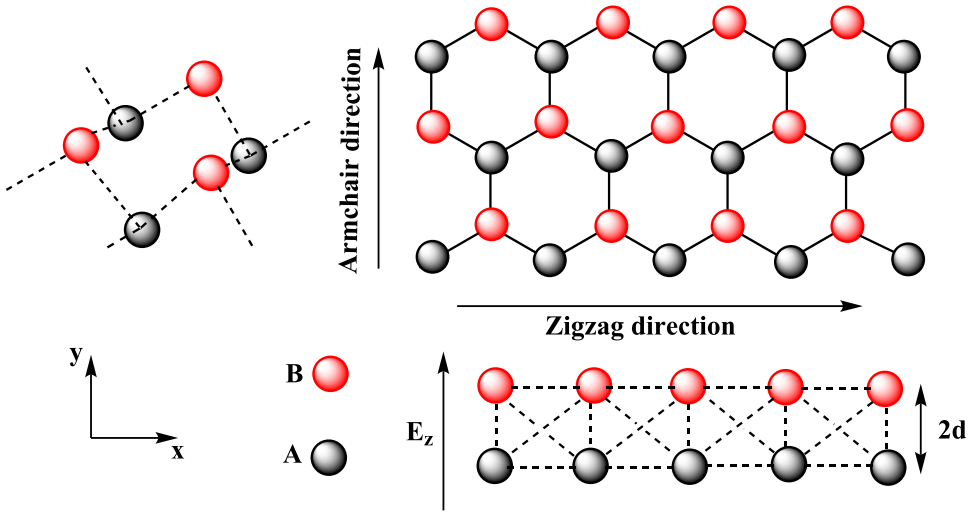

Fig. 1. Schematic illustration of silicene sheet. A and B sites separated by a distance $2d$ in the electric field E_z.

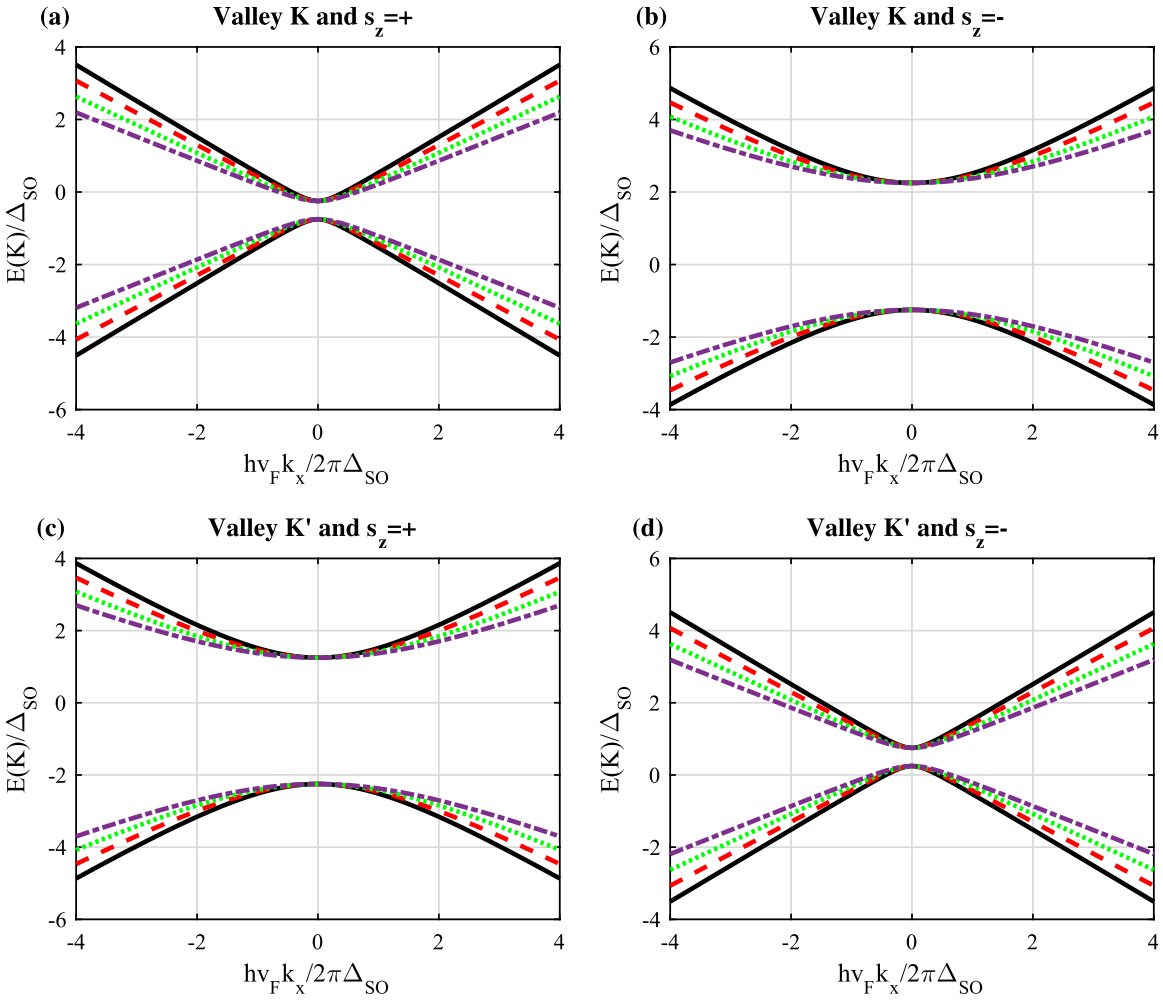

Fig. 2. (Colour online) The energy spectrum of ferromagnetic silicene with $M = \Delta_{SO}/2$ and $\Delta_z/\Delta_{SO} = 0.75$ for different strain modulus. $\epsilon = 0$ (black solid lines), $\epsilon = 5\%$ (red dashed lines), $\epsilon = 10\%$ (green dotted lines) and $\epsilon = 15\%$ (violet dotdashed lines).

EHC and MS of the system under strain and in Section 4, the numerical results are explained. Finally, Section 5 is the conclusion of the paper.

2. Theoretical formalism

In this section, we present the effective Hamiltonian model to describe the low-energy dynamics of carriers in a ferromagnetic silicene nanosheet which is subjected to a perpendicular uniform electric field as follows [18,42]

$$H_{\tau,s_z} = \hbar v_F (k_x \sigma_x - \tau k_y \sigma_y) - \tau s_z \Delta_{SO} \sigma_z + \Delta_z \sigma_z - M s_z \quad (1)$$

In our model, wave functions in the sublattice pseudospin space in

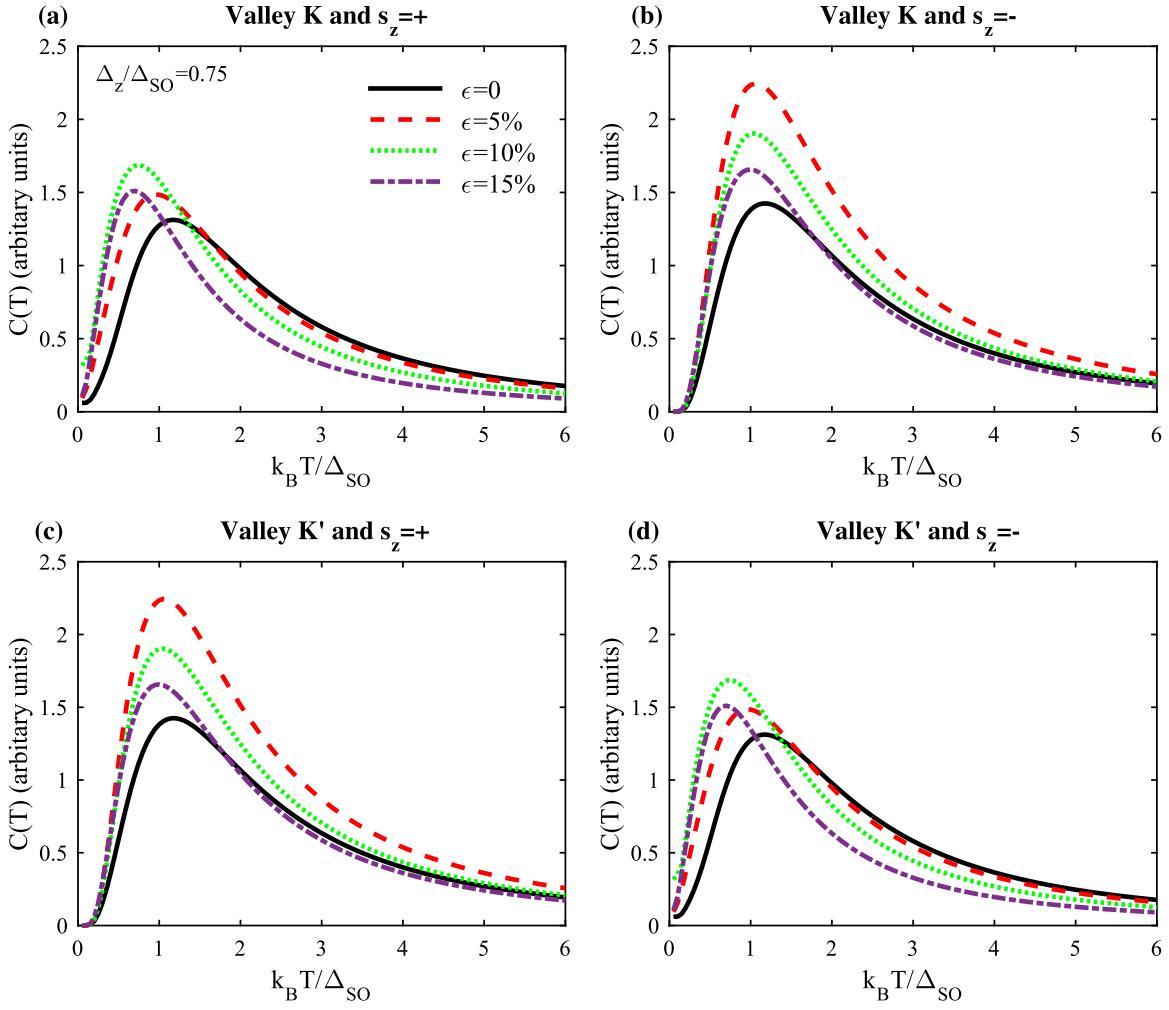

Fig. 3. Electronic heat capacity of ferromagnetic silicene with $M = \Delta_{SO}/2$ and $\Delta_z/\Delta_{SO} = 0.75$ for different strain modulus.

terms of the A and B sublattice components can be defined as $\Psi_{\tau,s_z} = \left\{\psi^A_{\tau,s_z}, \psi^B_{\tau,s_z}\right\}^T$. The first term is the normal graphene Hamiltonian (Dirac Hamiltonian) at Dirac cone approximation for valley $K(K')$ which are indexed by $\tau = +(-)$ and υ_F is the Fermi velocity of silicene at in-plane momentum $\mathbf{k} = (k_x, k_y)$ which is measured from the hexagonal first Brillouin zone. $\sigma_i (i = x, y, z)$ are the Pauli matrices. The second term is the Kane-Mele Hamiltonian for the intrinsic SO coupling, where for silicene $\Delta_{SO} = 3.9$ meV [18] and s_z is used for two spin degrees of freedom, up ($s_z = +$) and down ($s_z = -$). The third term referred to the on-site potential difference between A and B sublattices with $\Delta_z = E_z d$ in which E_z is the applied perpendicular electric field and $2d = 0.46$ nm is the vertical distance of sublattice's planes. You can see the Fig. 1. If silicene deposes on the surface of a magnetic insulator substrate, an exchange magnetization can be induced to the silicene with $M = \Delta_{SO}/2$ as exchange field [43,44]. The last term is due to this origin. The effect of strain on Hamiltonian is given by the two-dimensional reductions of the strain tensor as follows [31,45]

$$\varepsilon = \epsilon \begin{pmatrix} \cos^2\theta - \nu \sin^2\theta & (1+\nu)\cos\theta \sin\theta \\ (1+\nu)\cos\theta \sin\theta & \sin^2\theta - \nu \cos^2\theta \end{pmatrix} \tag{2}$$

In this equation, θ denotes the angle which the strain is applied with respect to the x axis direction, ϵ is the strain modulus and $\nu = 0.62$ is Poisson's ratio from *ab initio* calculations for silicene [46]. In our calculations $\theta = 0$ refer to strain along the ZZ direction. Therefore, we have considered our calculations based on the strain-induced and used converted nearest neighbors vectors. The model Hamiltonian under strain in Eq. (1) can be written as $H_{\tau,s_z}(\mathbf{K}) = U^\dagger(\theta) H^0_{\tau,s_z}(\mathbf{K}) U(\theta)$ wherein

$$U(\theta) = \begin{pmatrix} 1 & 0 \\ 0 & e^{-i\theta} \end{pmatrix},$$

is the unitary matrix performing a rotation in the sublattice space [47] and

$$H^0_{\tau,s_z}(\mathbf{k}) = \begin{pmatrix} \Delta_z - \tau s_z \Delta_{SO} - M s_z & \hbar\upsilon_F (k_x(1-\lambda_x\epsilon) + i\tau k_y(1 - \lambda_y\epsilon)) \\ \hbar\upsilon_F (k_x(1-\lambda_x\epsilon) - i\tau k_y(1-\lambda_y\epsilon)) & -\Delta_z + \tau s_z \Delta_{SO} - M s_z \end{pmatrix},$$

where $\lambda_x = 2.2$ and $\lambda_y = -1.3$ are the logarithmic derivative of the nearest-neighbor hopping with respect to the lattice parameter (a=0.386 nm) at $\epsilon = 0$ along the x and y directions, respectively [48]. However, the effective Hamiltonian is given by

$$H_{\tau,s_z}(\mathbf{k}) = \begin{pmatrix} \Delta_z - \tau s_z \Delta_{SO} - M s_z & \hbar\upsilon_F e^{-i\theta}(k_x(1-\lambda_x\epsilon) \\ & + i\tau k_y(1-\lambda_y\epsilon)) \\ \hbar\upsilon_F e^{i\theta}(k_x(1-\lambda_x\epsilon) - i\tau k_y(1-\lambda_y\epsilon)) & -\Delta_z + \tau s_z \Delta_{SO} - M s_z \end{pmatrix}. \tag{3}$$

Diagonalization of the above Hamiltonian leads to the following electronic bands

$$E_{\tau,s_z}(k) = \pm\sqrt{\Delta^2_{\tau,s_z} + (\hbar\upsilon_F k)^2} - M s_z \tag{4}$$

where $+(-)$ depicts the conduction (valance) bands, $\Delta_{\tau,s_z} = \Delta_z - \tau s_z \Delta_{SO}$

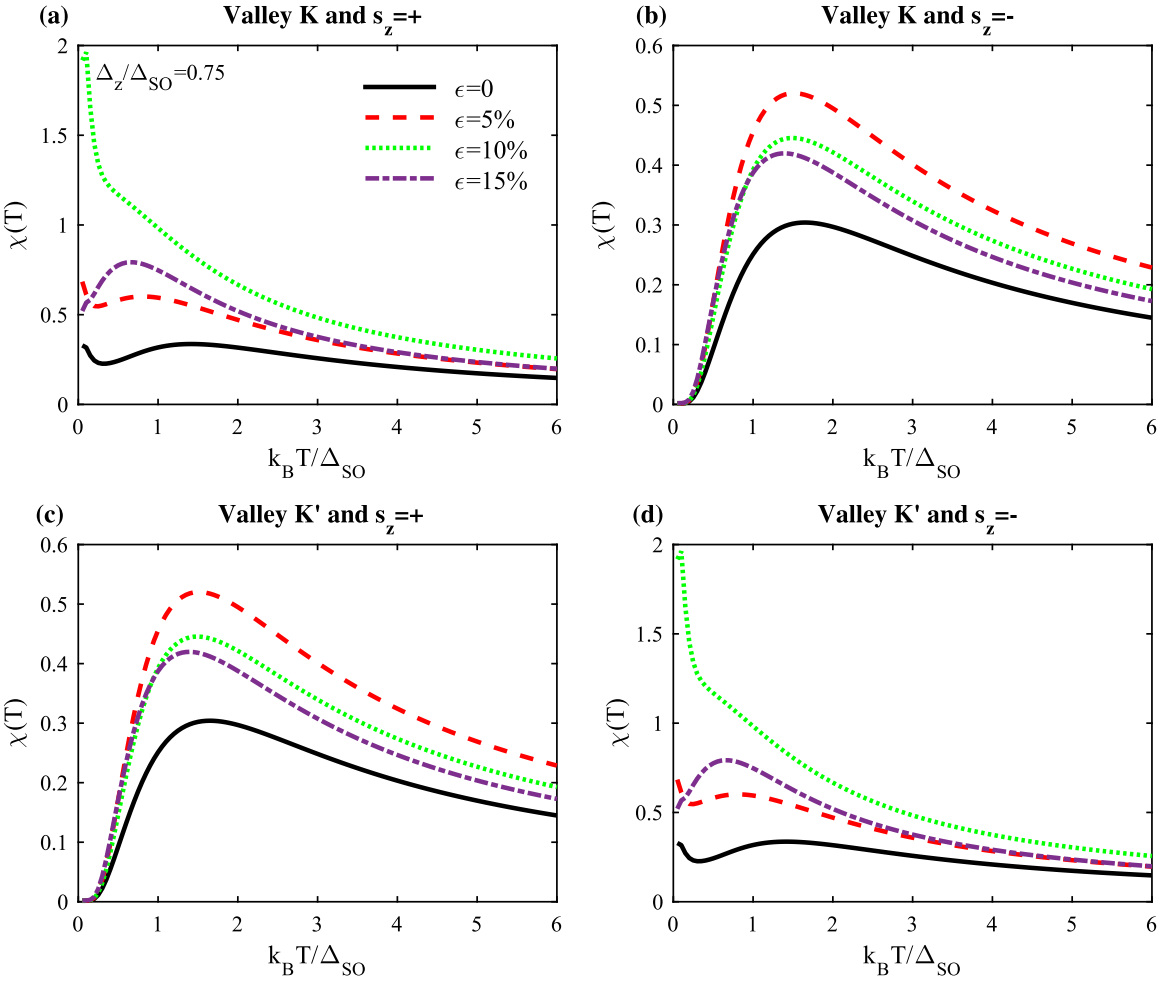

Fig. 4. Magnetic susceptibility of ferromagnetic silicene with $M = \Delta_{SO}/2$ and $\Delta_z/\Delta_{SO} = 0.75$ for different strain modulus.

and $k = \sqrt{k_{x'}^2 + k_{y'}^2}$ with $k'_x = k_x(1 - \lambda_x\epsilon)$ and $k'_y = k_y(1 - \lambda_y\epsilon)$. In the Matsubara formalism [49], each element of the Green's function matrix is defined by

$$G_{\alpha\beta}(\mathbf{k}, \gamma) = -\langle T_\gamma c_{k,\alpha}(\gamma) c^\dagger_{k,\beta}(0)\rangle G_{\alpha\beta}(\mathbf{k}, i\omega_n) = \int_0^{1/k_BT} e^{i\omega_n\gamma} G_{\alpha\beta}(\mathbf{k}, \gamma) d\gamma \tag{5}$$

where $c = a(b)$ and α, β refer to each sublattice atoms A and B and γ is the imaginary time. Also $\omega_n = (2n + 1)k_BT$ is the Fermionic Matsubara's frequency [49]. The Green's function matrix of the system $(\mathbf{G})$ can be readily obtained by the following equation

$$\mathbf{G}_{\tau,s_z}(\mathbf{k}, i\omega_n) = \frac{1}{i\omega_n \hat{\mathbf{I}} - H_{\tau,s_z}(\mathbf{k})} \tag{6}$$

After substituting Eq. (3) into Eq. (6), the Green's function matrix of this system can be found which is quite lengthy and has not been presented here. In the next section, EHC and MS of this system are calculated.

3. Electronic heat capacity and magnetic susceptibility

The DOS can be related to the trace over the imaginary part of Green's function, $D(E) = -\Im TrG(E)/\pi$. By taking trace based on the quantum numbers which label the Hamiltonian and by engaging Eqs. (3) and (6) and setting $i\omega_n \to E + i0^+$ as a numerical calculation in which 0^+ is a very small real number, the total DOS would straightforwardly be eventuated,

$$D(E) = -\frac{1}{2\pi N_c} \sum_{\mu,\mathbf{k}} \Im G_{\mu\mu}(\mathbf{k}, E + i0^+) \tag{7}$$

where μ describe a sub-site and N_c is the number of atoms in the unit cell. The EHC could be introduced by following expression [50]

$$C(T) = \int_{-\infty}^{+\infty} dE E D(E) \partial_T f(E) \tag{8}$$

in which $D(E)$ displays the DOS of Bloch electrons calculated by either of Eq. (7) and $f(E) = 1/[e^{E/k_BT} + 1]$ (k_B is the Boltzmann constant) represents the Fermi-Dirac distribution function. Calling Eqs. (7) and (8), the EHC would be obtained by,

$$C(T) = -\frac{1}{2\pi N_c T^2} \sum_{\mu,\mathbf{k}} \Im \int_{-\infty}^{+\infty} dE \frac{E^2 e^{E/k_BT}}{(e^{E/k_BT} + 1)^2} G_{\mu\mu}(\mathbf{k}, E + i0^+) \tag{9}$$

For a monolayer silicene lattice subjected to a perpendicular magnetic field, the MS can be written as [50,51]

$$\chi(T) = -\int_{-\infty}^{+\infty} dE D(E) \partial_E f(E) \tag{10}$$

Using Eqs. (7) and (10), the MS of the silicene lattice would be achieved as

$$\chi(T) = -\frac{1}{2\pi N_c T} \sum_{\mu,\mathbf{k}} \Im \int_{-\infty}^{+\infty} dE \frac{e^{E/k_BT}}{(e^{E/k_BT} + 1)^2} G_{\mu\mu}(\mathbf{k}, E + i0^+) \tag{11}$$

The study of $\chi(T)$ and $C(T)$ in the monolayer ferromagnetic silicene lattice constitutes the main aim in this work. In the next section, the results of EHC and MS are presented.

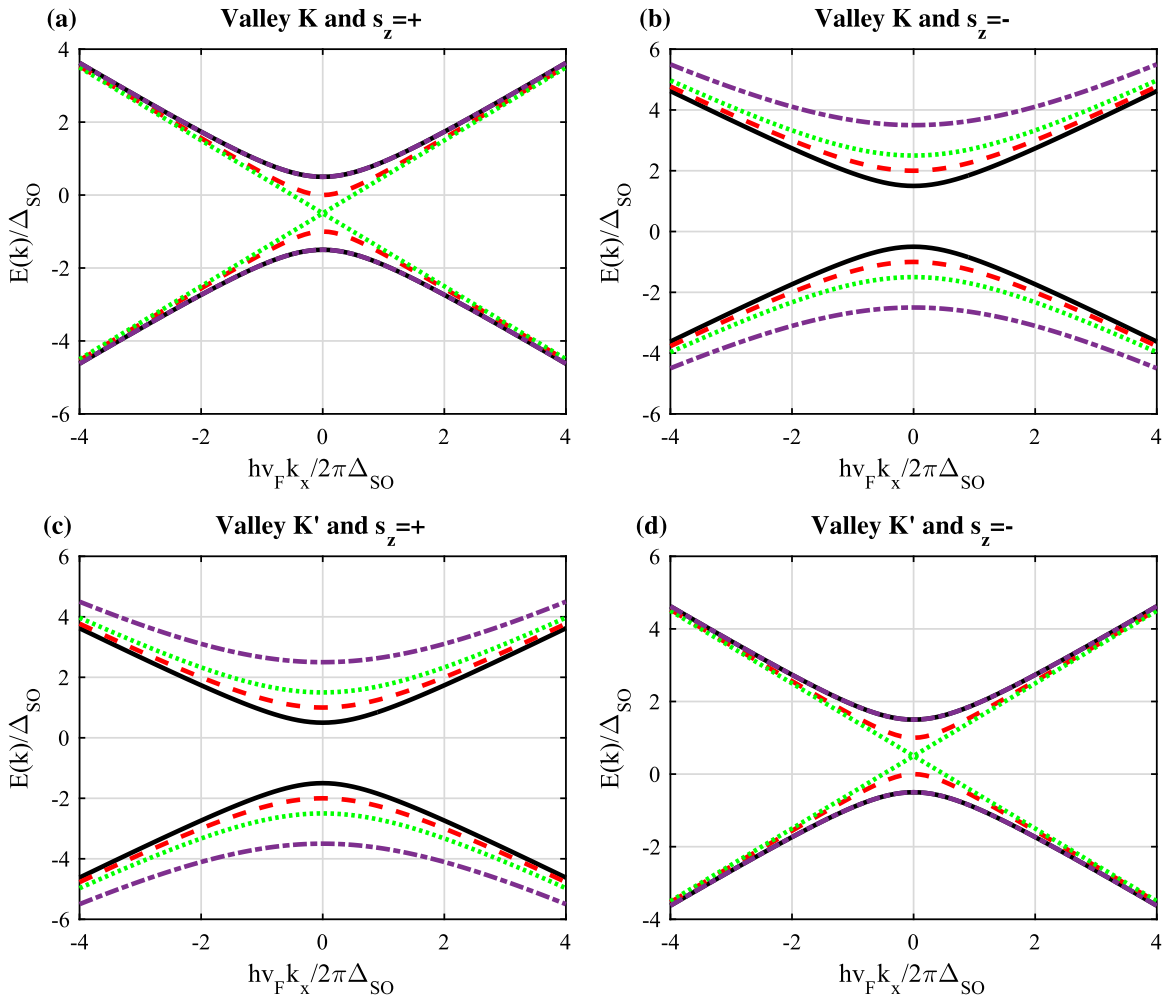

Fig. 5. (Colour online) The energy spectrum of ferromagnetic silicene with $M = \Delta_{SO}/2$ and $\epsilon = 7\%$ for different electric field strength ($E_z = \Delta_z/d$). $\Delta_z/\Delta_{SO} = 0$ (black solid lines), $\Delta_z/\Delta_{SO} = 0.5$ (red dashed lines), $\Delta_z/\Delta_{SO} = 1$ (green dotted lines) and $\Delta_z/\Delta_{SO} = 2$ (violet dotdashed lines).

4. Numerical results

Band structures of ferromagnetic silicene over the first Brillouin zone for $K(K')$ valleys under different strains, ϵ, with a fixed applied electric filed value, $\Delta_z/\Delta_{SO} = 0.75$, are shown based on Eq. (4) in Fig. 2. Also different kinds of spin configuration have considered. Because of the unique band structure of silicene, a symmetry between valleys and their spins has been seen. Plots are reflected with respect to $E(k)/\Delta_{SO} = 0$ by exchanging the spin up and down. The $\epsilon = 0$ (black solid lines), $\epsilon = 5\%$ (red dashed lines), $\epsilon = 10\%$ (green dotted lines) and $\epsilon = 15\%$ (violet dotdashed lines) are the various values of the strain modulus. In the presence of an applied external electric field, the slope of bands decreases with strain for the whole kinds of configurations, which leads to the increasing of electron and hole effective masses and transport decreases. Also non-vanishing density of states at Fermi energy is found. Surprisingly, the direct band gap due to the breaking of inversion symmetry remains at the Fermi level and the system is a semimetal for all strains in the presence of electric field which is in qualitative agreement with results of recent works [20,52]. This can be understood from the fact that the potentials seen by the silicon atoms at the A and B sublattices are different. In other studies a semimetal-metal transition has been seen in the absence of electric field [53,54]. As a point, spin splitting for $\Delta_z/\Delta_{SO} = 0.75$ ($\Delta_z < \Delta_{SO}$) has been occurred in Figs. 2(a) and (b) for valley K and Figs. 2(c) and (d) for valley K' which has consistence with the results of Nicol and Tabert [55]. These behaviors can be affected the temperature behavior of EHC and MS of the system.

Now, by the confirmed band structure results, the investigation of EHC and MS is easier. It is well-known that the EHC of semiconductors, in the low temperature, can be written as $C(T) \propto e^{-\Delta/T}$ [50,56]. According to this formula, with decreasing the gap, the EHC increases in the low temperature region as it is shown in Fig. 3 for all cases. Because of the symmetry between valleys, we focus on the valley K with spin up and down, which the results are the same for valley K' with spin down and up, respectively. As we can see, the EHC decreases in the high temperature region. Figs. 3(a) and (d) illustrate a crossover in the heat capacity of the system known as Schottky anomaly in the presence of electric field and strain. By increasing the strain, band structure becomes flat and the mass of carriers is larger than the unstrained case. This leads to the increasing of the Schottky anomaly and appears over a small range of temperatures when thermal energy reaches to the energy gap between the sub-bands. As a result, around $k_BT/\Delta_{SO} < 1$, EHC increases with strain, while for temperatures $k_BT/\Delta_{SO} > 1$, it decreases. For Figs. 3(a)-(d), Schottky anomaly slightly moves to the lower temperatures and EHC changes with respect to a critical strain ($\epsilon = 10\%$). For the cases (a) and (d), this value gives the maximum EHC, while for (b) and (c), before (after) this value, EHC is maximum (minimum), respectively. This critical strain shows its behavior better in the temperature dependence of MS in Figs. 4(a) and (d). At very low (high) temperatures, MS diverges (vanishes), respectively. At high temperatures, quantum effects are too weaker than thermal effects and changing the strain does not affect the temperature behavior of MS and all curves fall on each other. Also for the critical strain in the presence of electric field, MS is maximum. Moreover, the crossover is

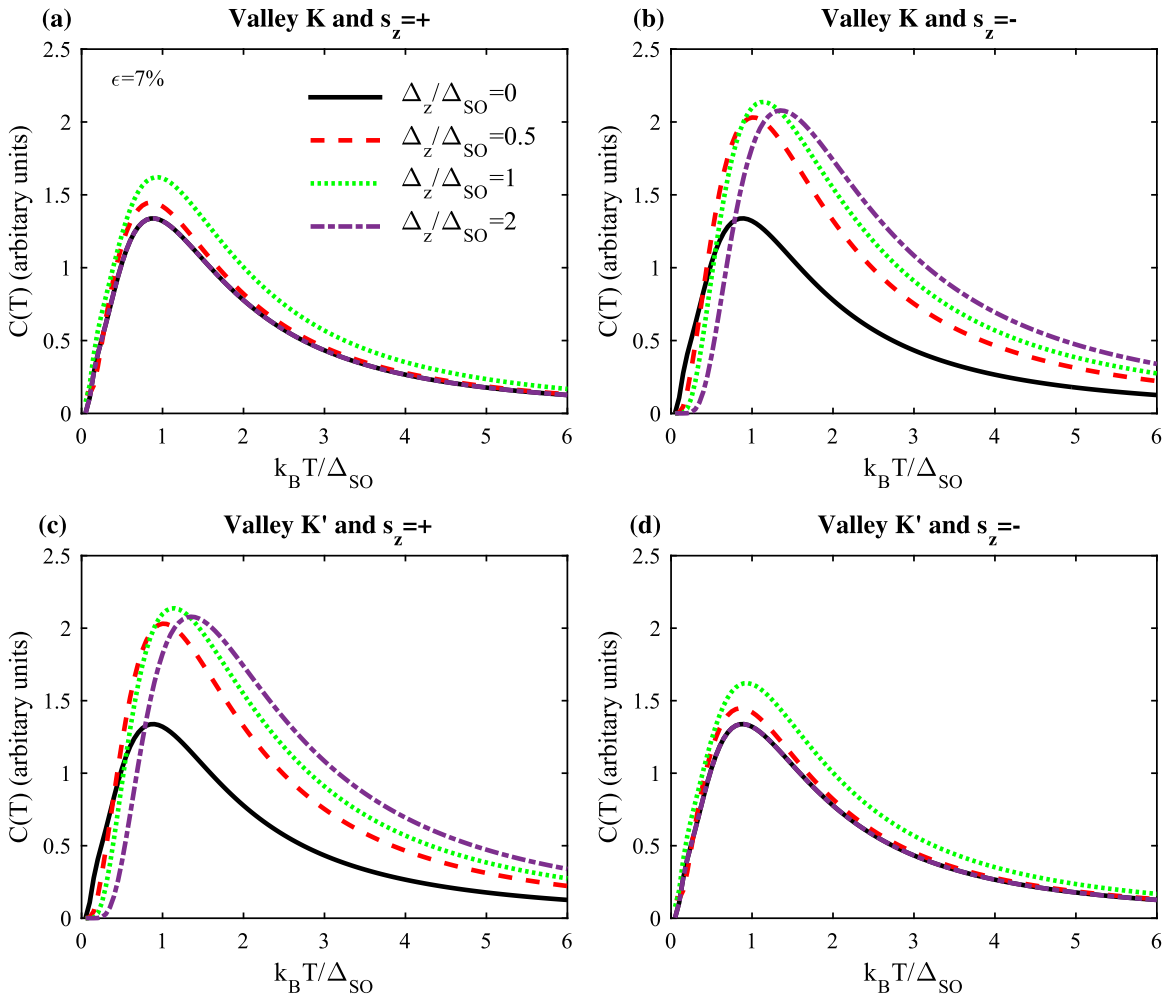

Fig. 6. Electronic heat capacity of ferromagnetic silicene with $M = \Delta_{SO}/2$ and $\epsilon = 7\%$ for different electric field strength ($E_z = \Delta_z/d$).

disappeared in this value of strain and a decreasing behavior is found. A crossover appears around $k_BT/\Delta_{SO} \approx 1.5$ and the behavior of $\chi(T)$ is different before and after that. $\chi(T)$ increases (decreases) with temperature before (after) the crossover. Before the crossover, when the temperature decreases, the magnetic ordering reduces due to quantum fluctuations. After the crossover, thermal fluctuations are more important than quantum fluctuations and the susceptibility decreases in high temperatures thus the behavior with strain is the same with $C(T)$.

A plot of the band structure evolution around the K and K' points for increased Δ_z/Δ_{SO} is shown in Fig. 5. Because of the symmetry between valleys, at the K' point, the spin labels switch. For $\Delta_z/\Delta_{SO} = 0$, in the presence of the strain about $\epsilon = 7\%$, spin degeneration of all energy bands has been broken and separated by an insulating gap of Δ_{SO} (black solid lines). By increasing of the electric field for $\Delta_z < \Delta_{SO}$, the system behavior is similar to a topological insulator (TI) and the system has two different behavior for spin up and down at K and K' valleys. For spin up (down) at $K(K')$, the gap decreases and for spin down (up) at $K(K')$, the gap increases with Δ_z/Δ_{SO}. When Δ_z reaches to the Δ_{SO}, i.e., $\Delta_z = \Delta_{SO}$, the band gap closes and as Δ_z is increased further, a transition to the band insulator phase has occurred and then band gap reopens, which is in agreement with the mentioned work by Nicol and Tabert. It is necessary to say that this occurs only for valley $K(K')$ with spin up (down) and this transition has a main role in studying of transport properties. For valley $K(K')$ with spin down (up), the band gap slightly increases with electric field.

According to these explanations and the confirmation of the results, the temperature dependence of EHC and MS are investigated. For valley $K(K')$ with spin up (down) in the presence of strain about $\epsilon = 7\%$, the transition to the TI regime for $\Delta_z < \Delta_{SO}$ increase the Schottky anomaly as reaches to the its maximum value for $\Delta_z = \Delta_{SO}$ at $k_BT/\Delta_{SO} = 1$ and then decreases due to the transition to the band insulator for $\Delta_z > \Delta_{SO}$, as shown in Figs. 6(a) and (d). For Figs. 6(b) and (c), the EHC has the behavior as $C(T) \propto e^{-\Delta/T}$, but when we increase the electric field, it slightly increases due to the increasing of the band gap in Figs. 5(b) and (c) and the Schottky anomaly moves to the higher temperatures. In fact, the higher energy is need to conductance at large induced electric fields due to the increasing of the scattering rate. It is necessary to note that the EHC decreases (increases) with the electric field at low (high) temperatures. As a consequence, in Figs. 7(a) and (d), MS has a decreasing behavior for TI phase and since the thermal effects are dominant at high temperatures, all curves fall on each other. Also it increases (decreases) before (after) the crossover at $k_BT/\Delta_{SO} = 1$. In other words, when the induced energy due to the temperature is smaller than the SO coupling, MS increases because of the relation $\chi(T) \propto T^{-1}e^{-E_g/k_BT}$ which here E_g is due to the applied electric field and after that decreases. The same behavior, but with a softer slope is found with respect to the $C(T)$ for Figs. 7(b) and (c).

5. Conclusions

To sum up, Green's function approach has been performed to study the low energy electronic structure and thermodynamic properties of a ferromagnetic silicene under strain in the presence of electric field. For silicene at a fixed electric field, spin band gaps does not change with the strain along the zigzag direction, but EHC and MS changes in two

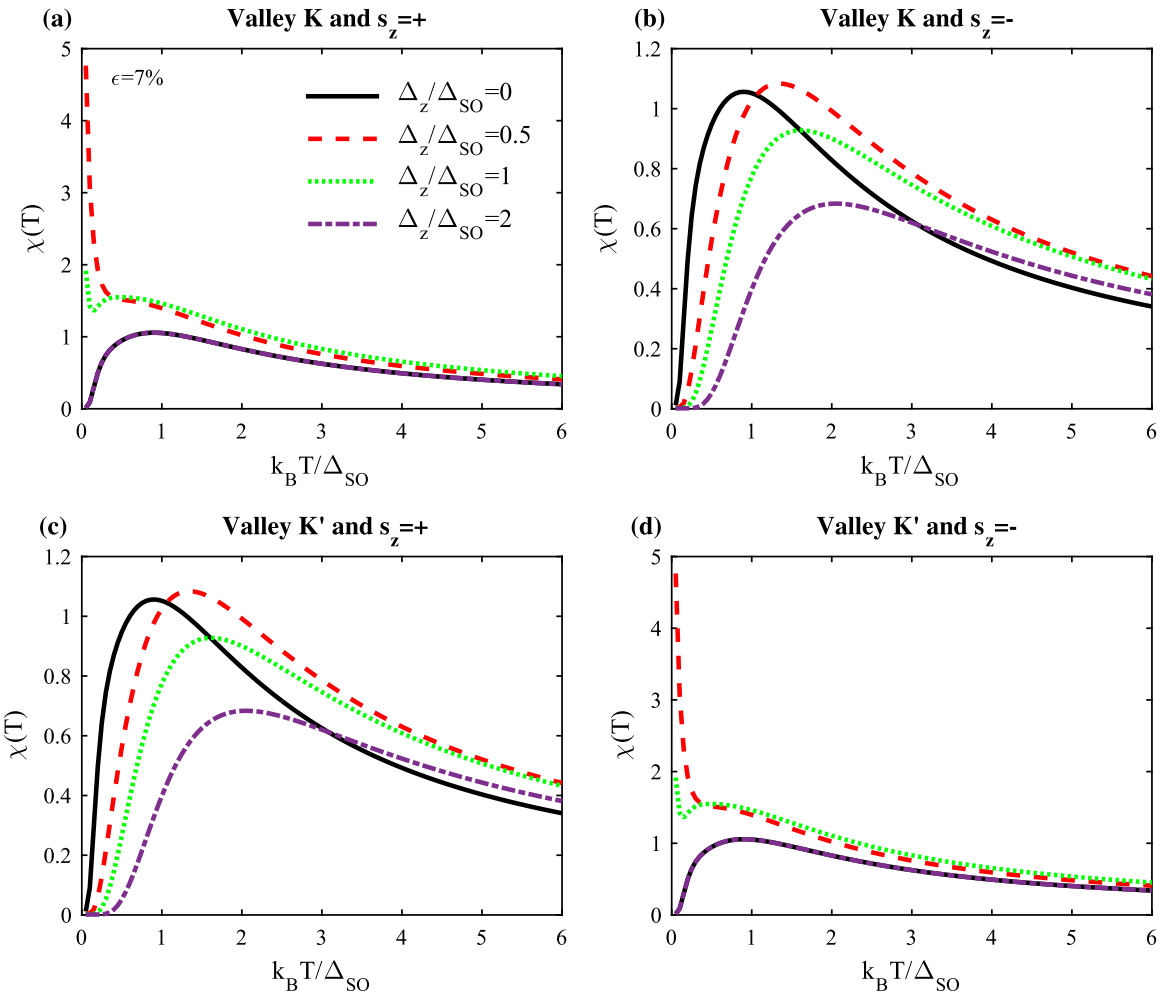

Fig. 7. Magnetic susceptibility of ferromagnetic silicene with $M = \Delta_{SO}/2$ and $\epsilon = 7\%$ for different electric field strength ($E_z = \Delta_z/d$).

temperature regions as there is a critical strain about 10%. However, electric field affects the spin band gaps of ferromagnetic silicene under strain and a transition to the topological insulator occurs which affects the temperature behavior of EHC and MS. In all of the temperature regions, the electric field and strain causes the enhancement of Schottky anomaly in the EHC and a crossover in the MS curves appears at low temperatures.

References

[1] K.S. Novoselov, A.K. Geim, S.V. Morozov, D. Jiang, Y. Zhang, S.V. Dubonos, I.V. Grigorieva, A.A. Firsov, Science 306 (2004) 666.
[2] K.F. Mak, C. Lee, J. Hone, J. Shan, T.F. Heinz, Phys. Rev. Lett. 105 (2010) 136805.
[3] A.H. Castro Neto, F. Guinea, N.M.R. Peres, K.S. Novoselov, A.K. Geim, Rev. Mod. Phys. 81 (2009) 109.
[4] N.M.R. Peres, Rev. Mod. Phys. 82 (2010) 2673.
[5] M. Yarmohammadi, J. Electron. Mater. 45 (2006) 4958.
[6] K.S. Novoselov, D. Jiang, F. Schedin, T.J. Booth, V.V. Khotkevich, S.V. Morozov, A.K. Geim, Proc. Natl. Acad. Sci. Usa. 102 (2005) 10451.
[7] G.W. Semenoff, Phys. Rev. Lett. 53 (1984) 2449.
[8] M. Yarmohammadi, M. Zareyan, Chin. Phys. B 25 (2016) 068105.
[9] M.I. Katsnelson, K.S. Novoselov, A.K. Geim, Nat. Phys. 2 (2006) 620.
[10] Y. Lin, K.A. Jenkins, A. Valdes-Garcia, J.P. Small, D.B. Farmer, P. Avouris, Nano Lett. 9 (2009) 422.
[11] J. Kedzierski, P. Hsu, P. Healey, P.W. Wyatt, C.L. Keast, M. Sprinkle, C. Berger, W.A. de Heer, IEEE Trans. Electron Devices 55 (2008) 2078.
[12] B. Lalmi, H. Oughaddou, H. Enriquez, A. Kara, S. Vizzini, B. Ealet, B. Aufray, Appl. Phys. Lett. 97 (2010) 223109.
[13] P.E. Padova, C. Quaresima, C. Ottaviani, P.M. Sheverdyaeva, P. Moras, C. Carbone, D. Topwal, B. Olivieri, A. Kara, H. Oughaddou, B. Aufray, G.L. Lay, Appl. Phys. Lett. 96 (2010) 261905.
[14] B. Aufray, A. Vizzini, H. Oughaddou, C. Lndri, B. Ealet, G.L. Lay, Appl. Phys. Lett. 96 (2010) 183102.
[15] P. Vogt, P. De Padova, C. Quaresima, J.A.E. Frantzeskakis, M.C. Asensio, A. Resta, B. Ealet, G.L. Lay, Phys. Rev. Lett. 108 (2012) 155501.
[16] N.D. Drummond, V. Z'olyomi, V.I. Fal'ko, Phys. Rev. B 85 (2012) 075423.
[17] Z. Ni, Q. Liu, K. Tang, J. Zheng, J. Zhou, R. Qin, Z. Gao, D. Yu, J. Lu, Nano Lett. 12 (2012) 113.
[18] C.-C. Liu, W. Feng, Y. Yao, Phys. Rev. Lett. 107 (2011) 076802.
[19] N.D. Drummond, V. Z'olyomi, V.I. Fal'ko, Phys. Rev. B 85 (2012) 075423.
[20] M. Ezawa, New J. Phys. 14 (2012) 033003.
[21] M. Ezawa, Phys. Rev. Lett. 109 (2012) 055502.
[22] X.-T. An, Y.-Y. Zhang, J.-J. Liu, S.-S. Li, New J. Phys. 14 (2012) 083039.
[23] M. Tahir, U. Schwingenschlogl, Sci. Rep. 3 (2013) 1075.
[24] M. Ezawa, Phys. Rev. Lett. 110 (2013) 026603.
[25] W.-F. Tsai, C.-Y. Huang, T.-R. Chang, H. Lin, H.-T. Jeng, A. Bansil, Nat. Commun. 4 (2013) 1500.
[26] C.J. Tabert, E.J. Nicol, Phys. Rev. Lett. 110 (2013) 197402.
[27] H. Pan, Z. Li, C.-C. Liu, G. Zhu, Z. Qiao, Y. Yao, Phys. Rev. Lett. 112 (2014) 106802.
[28] G. Gui, J. Li, J. Zhong, Phys. Rev. B 78 (2008) 075435.
[29] V.M. Pereira, A.H. Castro Neto, N.M.R. Peres, Phys. Rev. B 80 (2009) 045401.
[30] S.-M. Choi, S.-H. Jhi, Y.-W. Son, Phys. Rev. B 81 (2010) 081407 (R).
[31] M. Farjam, H. Rafii-Tabar, Phys. Rev. B 80 (2009) 167401.
[32] G. Liu, M.S. Wu, C.Y. Ouyang, B. Xu, Eur. Lett. 99 (2012) 17010.
[33] Y. Wang, Y. Ding, Solid State Commun. 155 (2013) 6.
[34] T.P. Kaloni, Y.C. Cheng, U. Schwingenschlogl, J. Appl. Phys. 113 (2013) 104305.
[35] B. Mohan, A. Kumar, P.K. Ahluwalia, Physica E 61 (2014) 40.
[36] H. Zhao, Phys. Lett. A 376 (2012) 3546.
[37] E. Scalise, M. Houssa, G. Pourtois, B. Broek, V. Afanasev, A. Stesmans, Nano Res. 6 (2013) 19.
[38] H.P. Li, R.Q. Zhang, EPL 99 (2012) 36001.
[39] M. Hu, X. Zhang, D. Poulikakos, Phys. Rev. B 87 (2013) 195417.
[40] Q.-X. Pei, Y.-W. Zhang, Z.-D. Sha, V.B. Shenoy, J. Appl. Phys. 114 (2013) 033526.
[41] T.Y. Ng, J. Yeo, Z. Liu, Int. J. Mech. Mater. Des. 9 (2013) 105.
[42] T. Yokoyama, Phys. Rev. B 87 (2013) 241409.
[43] H. Haugen, D. Huertas-Hernando, A. Brataas, Phys. Rev. B 77 (2008) 115406.
[44] Z. Qiao, S.A. Yang, W. Feng, W.-K. Tse, J. Ding, Y. Yao, J. Wang, Q. Niu, Phys. Rev. B 82 (2010) 161414.
[45] V.M. Pereira, A.H. Castro Neto, N.M.R. Peres, Phys. Rev. B 80 (2009) 045401.
[46] B. Wang, J. Wu, X. Gu, H. Yin, Y. Wei, R. Yang, M. Dresselhaus, Appl. Phys. Lett.

104 (2014) 081902.
[47] F.M.D. Pellegrino, G.G.N. Angilella, R. Pucci, Phys. Rev. B 85 (2012) 195409.
[48] F. Sattari, J. Magn. Magn. Mater. 414 (2016) 19.
[49] G.D. Mahan, Many Particle Physics, Plenum Press, New York, 1993.
[50] C. Kittle, Introduction to Solid State Physics, eighth ed., Wiley, New York, 2004.
[51] W. Nolthing, A. Ramakanth, Quantum Theory of Magnetism, Springer, New York, 2009.
[52] X. Lin, J. Ni, J. Appl. Phys. 117 (2015) 164305.
[53] B. Rakshit, P. Mahadevan, Phys. Rev. B 82 (2010) 153407.
[54] R. Qin, Ch. Wang, W. Zhu, Y. Zhang, AIP Adv. 2 (2012) 022159.
[55] C.J. Tabert, E.J. Nicol, Phys. Rev. B 88 (2013) 085434.
[56] R.K. Pathria, Statistical Mechanics, Oxford Press, London, 1997.